



# Interconnected Autonomous AC Microgrids via Back-to-Back Converters—Part I: Small-Signal Modeling

Mobin Naderi, *Student Member, IEEE*, Yousef Khayat, *Student Member, IEEE*, Qobad Shafiee, *Senior Member, IEEE*, Tomislav Dragicevic, *Senior Member, IEEE*, Hassan Bevrani, *Senior Member, IEEE*, and Frede Blaabjerg, *Fellow, IEEE*

**Abstract**—In this paper, a set of autonomous AC Microgrids interconnected by back-to-back converters is taken into account, where they are supplied fully using voltage source converter-based distributed energy resources. A comprehensive and generalized small-signal model of the interconnected autonomous microgrids as a large-scale system is proposed using the interconnection method. The modeling is based on detailed module models to show the impact of each module on the dynamic modes, especially the dominant critical modes. It is generalized and scalable due to separate modeling of modules as well as using unlimited and expandable interconnecting. The proposed interconnection method deals with all electrical and control connections between individual modules including feed-back, feed-forward, augmentation, and the order of module inputs and outputs. The model is validated employing Prony analysis method and using output results of an OPAL-RT real-time simulator. Using the proposed modeling method, the small-signal stability analysis and controller design can be realized simply for interconnected microgrids with any number of microgrids and different structures. Typically for two interconnected microgrids, all dynamic modes and participant state variables in different frequency ranges are identified using the eigenvalue analysis and participation matrix in MATLAB.

**Index Terms**—Back-to-back converters, eigenvalue analysis, interconnected AC microgrids, small-signal modeling, state space representation.

## I. INTRODUCTION

INDIVIDUAL Microgrids (MGs) are independent units of modern power grids, which integrate distributed energy resources (DERs) and localize the production and consumption of electricity. Each MG consists of a group of DERs, storage systems, loads, as well as protection and control devices that can be operated in both grid-connected and autonomous modes. MGs improve the stability, reliability, economic optimality and resiliency in comparison with individual DERs and provide auxiliary services for conventional distribution systems [1]–[3]. Although, the need for improving security, reliability, sustainability, flexibility and DER penetration level of individual MGs leads to the solution of networking [3]. If interconnected microgrids (IMGs) are operated stable and

optimal, they can give many advantages to local consumers and distribution systems.

IMGs can be constructed in various structures. AC/DC MGs, AC/DC interlinking lines (ILs), interlinking devices, type of interconnecting and control, as well as communication methods lead to different IMG structures [4]. Fully DC IMGs interconnected by DC ILs [5], [6], fully AC IMGs interconnected through AC ILs [7]–[12], and mixed DC and AC IMGs interconnected through DC/AC ILs and DC-AC converters [13] are presented in the literature. AC MGs are more taken into account due to their challenges in voltage and frequency controls, both active and reactive power exchanges and the correspondence with the present AC distribution networks, which can be clustered into AC IMGs and form a new operating IMG mode.

In order to interconnect AC MGs, back-to-back converters (BTBCs), circuit breakers (CBs) and static switches can be used as interlinking devices. CBs and instantaneous static switches are used as interlinking devices in [7], [8], [10], [12], [14]–[16] that can only network AC MGs with the same nominal voltages and frequencies. In such IMGs (named by CB-IMGs) a synchronizing algorithm is required to interconnect MGs. Power exchange/sharing can be controlled by changing droop coefficients of primary controllers [7], adding a signal to secondary controllers [12], [15] or employing hierarchical control [14]. More flexible power exchange can be achieved by networking AC MGs using BTBCs [9], [11], [17]–[19]. Moreover, independently control of frequency and voltage of each MG [18], [20], power quality improvement by reactive/harmonic power interchange control [19], and integration of multiple AC MGs with different nominal voltages/frequencies [17], [18] can be addressed for IMGs via BTBCs (called BTBC-IMGs). In addition, several applications of BTBCs for bidirectional power flow between MGs and the utility grid are reported [21], [22].

Small-signal modeling is a well-known method to understand the behaviour of systems around an equilibrium point. It is engaged for autonomous MGs performance and stability analysis as well as controller design [23]–[28]. In the case of IMGs, the presented small-signal models are generally an expansion of [23]. A special configuration of MGs is considered in [9], which any MG has a STATCOM to be coordinated with power exchanging BTBC. Then, an eigenvalue analysis and a robust distributed controller design are done based

M. Naderi, Y. Khayat, Q. Shafiee, and H. Bevrani are with the Smart/Micro Grids Research Center (SMGRC), University of Kurdistan, Sanandaj, Iran, P.C.: 66177-15175. E-mail: (m.naderi@eng.uok.ac.ir, y.khayat@eng.uok.ac.ir, q.shafiee@uok.ac.ir, and bevrani@eng.uok.ac.ir), website: <https://smgrc.uok.ac.ir/>. T. Dragičević and F. Blaabjerg are with the Department of Energy Technology, Aalborg University, Aalborg, DK, 9220, Denmark. E-mail: (tdr@et.aau.dk, and fbl@et.aau.dk).

on the small-signal model, while BTBC modeling has not been addressed. Another modeling of BTBC-IMGs refers to multiple MGs connected to an ideal main grid, where a lower challenging structure of IMGs is concerned with respect to the grid-isolated IMGs [21]. A detailed small-signal modeling is developed for CB-IMGs and is simplified using a truncation order reduction model [10]. Another detailed model for fully PV-based CB-IMGs is obtained in order to find oscillating modes and increase their damping [15]. An aggregation-based simplified model is presented recently, which finds a reduced-order model for CB-IMGs in low-frequency and medium-frequency dynamics [29]. More CB-IMGs are analyzed in order to define suitable range of electrical and control parameters such as interlinking line length and droop gains [10], [15], [16], [30], as well as to analyze power exchange control performance [12], [14], [31].

This paper develops an easily generalized small-signal modeling method for BTBC-IMGs in the absence of a stiff main grid. Distinctive features of this paper can be listed as follows.

- Unlike all existing modeling methods for IMGs, a detailed comprehensive method is proposed, which is simply generalized for any number of MGs and interlinks by applying the interconnection method.
- In the proposed interconnection method, each module is modeled separately by a state space representation, then its connections with other modules are considered in the input and output. Interconnection process will be completed without any analytical calculation and merely using valuable functions of Robust Control Toolbox (RCT) in MATLAB, which strongly decreases calculation burden/error.
- Opposed to the existing method in [14], [15], which needs many substitutions to obtain interconnections between modules, the proposed interconnection method is much simpler in calculation due to computing all electrical and control connections between individual modules employing RCT functions. Therefore, the overall IMG modeling is facilitated even for large ones.
- In the proposed modeling method for IMGs, the BTBCs are included as interlinking devices, which are not taken into account in the literature [9], [10], [12], [14]–[16], [31].
- Similar to some validation methods for power systems [32], [33], the proposed interconnection method is validated using Prony method, which compares each state variable with its waveform simulated in OPAL-RT real-time simulator.
- Impact of the most effective state variables and corresponding parameters on the dominant modes of IMGs are recognized, which will show a remarkable effect of BTBCs on the IMG stability.

The rest of this paper is organized as follows. An overview of the control structure and requirements is addressed in Section II. Section III presents a comprehensive modeling method for BTBC-IMGs, including modeling of individual MGs, ILs, BTBCs and their interconnection. In Section IV, the proposed method is validated using Prony analysis and

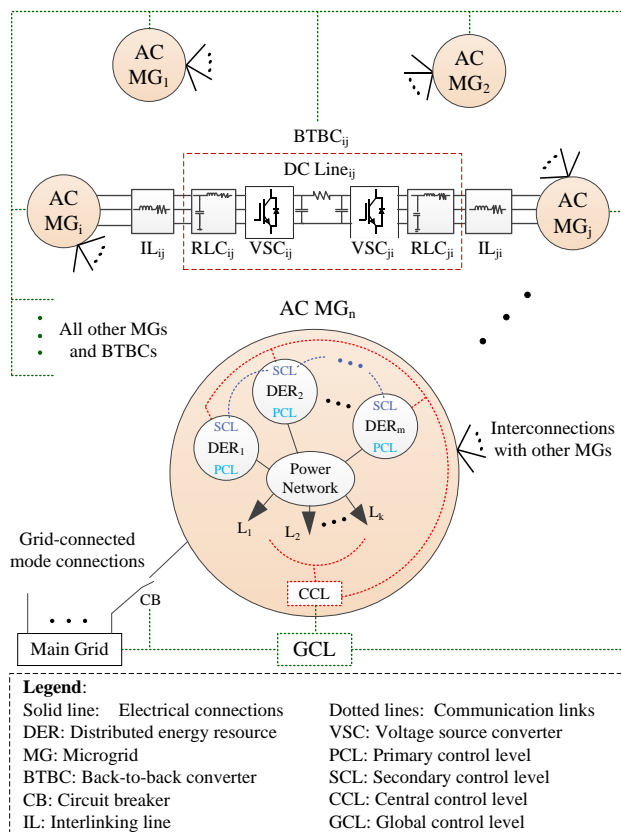


Fig. 1. AC interconnected microgrids using back-to-back converters, DC and AC interlinking lines for physical interconnection and the four-level hierarchical control for control interconnection.

OPAL-RT real-time simulator. Eigenvalue analysis results are reported in Section V. Finally, the conclusion is given in Section VI.

## II. CONTROL STRUCTURE AND REQUIREMENTS

Fig. 1 shows a general structure of AC IMGs, including autonomous MGs, AC and DC ILs, and BTBCs as the main components. The MGs may have different structures with any number of DERs, loads and lines, which are interconnected using BTBCs, and AC/DC ILs.

A four-level hierarchical control presented in [1] is considered here to take the control responsibility of MGs in both individual and interconnected operating modes. The primary control level (PCL) comprises decentralized droop controllers implemented for each DER cascading with inner voltage and current controllers. The vital objectives of voltage/frequency stability, active/reactive power sharing and current limiting are fulfilled in the PCL. The secondary control level (SCL) is mainly responsible for voltage/frequency restoration and power sharing improvement. However, some ancillary objectives such as power quality improvement may be done in the SCL. The most common architectures for the SCL are centralized and distributed types, where communication links are used to share the data among DERs. The central control level (CCL) provides the supervisory MG capabilities, e.g. grid connecting and load shedding. The high-level energy/power management is done in the global control level (GCL). The optimal power flow among IMGs or among individual MGs

and the main grid is accomplished in the GCL by communicating the production and consumption data of all participants.

In this paper, the PCL is applied to each DER, which is only active MG control loop during a small-signal disturbance. In fact, The SCL is considered to act after the primary control [28], [34], when the dynamics of the disturbance and the PCL are finished. Therefore, the SCL dynamics are not considered. Moreover, since the CCL functions, e.g. emergency control are not interested to be studied here except the coordination control, they are not included. Nevertheless, the impact of SCL and CCL dynamics on the IMG stability can be studied in future works. In the IMG operating mode, the GCL role can be divided into two parts: 1) an optimization process based on the communicated data and 2) sending set-points to control units including the CCLs and BTBCs as shown in Fig. 1. The first duty is out of the paper studies while the second one is considered to be well established. It is due to the fact that the GCL time-scale (minutes to an hour) and the CCL time-scale (a few minutes) in sending set-points are separated from the desired dynamics (seconds or fraction of a second). In other words, the CCL and BTBC set-points sent by the GCL and the set-points sent from the CCL to the downstream controllers are permanent during small-signal disturbances.

It is noteworthy to mention that the coordination among all IMGs and BTBCs is according to the GCL set-points. Let us assume that a power shortage is reported to the GCL by  $MG_i$  in a specific time span. The amount of power flow to  $MG_i$ , the number of involved BTBCs and MGs as well as MG commitment are determined by the optimal power flow management in the GCL. Hence, the GCL set-points sent to all control units result in a coordinated operation for IMGs. Communicating the data in all levels is considered ideal, i.e. without dynamics.

Note that the grid-connected mode is not considered in this paper in order to focus on the stability analysis of the weak MGs interconnected by BTBCs. In addition, the IMG operating mode can be a new flexible mode, which needs to be studied in terms of stability, control, reliability and resiliency.

### III. SMALL-SIGNAL MODELING OF INTERCONNECTED MICROGRIDS

#### A. Interconnection method for Interconnected Microgrids

The schematic of AC IMGs in a general form is shown in Fig. 1. In order to have a comprehensive and easily generalized model of IMGs, similar modules are modeled in the same format. Then, the modeling process is divided into two main steps: 1) modeling of each module separately and 2) interconnecting all the modules using the interconnection method.

Fig. 2 shows the modeling process including both steps. The main modules consists of islanded AC MGs, AC ILs and BTBCs. DC ILs are modeled as a part of BTBCs. Once all  $M$  modules are modeled separately in the first step, the interconnection method is applied to interconnect them in the second step. Note that Fig. 2 is also a guideline for the presented interconnection method in Section III.

In the interconnection method, each module i.e. an MG, a BTBC or an AC IL is represented individually by a state

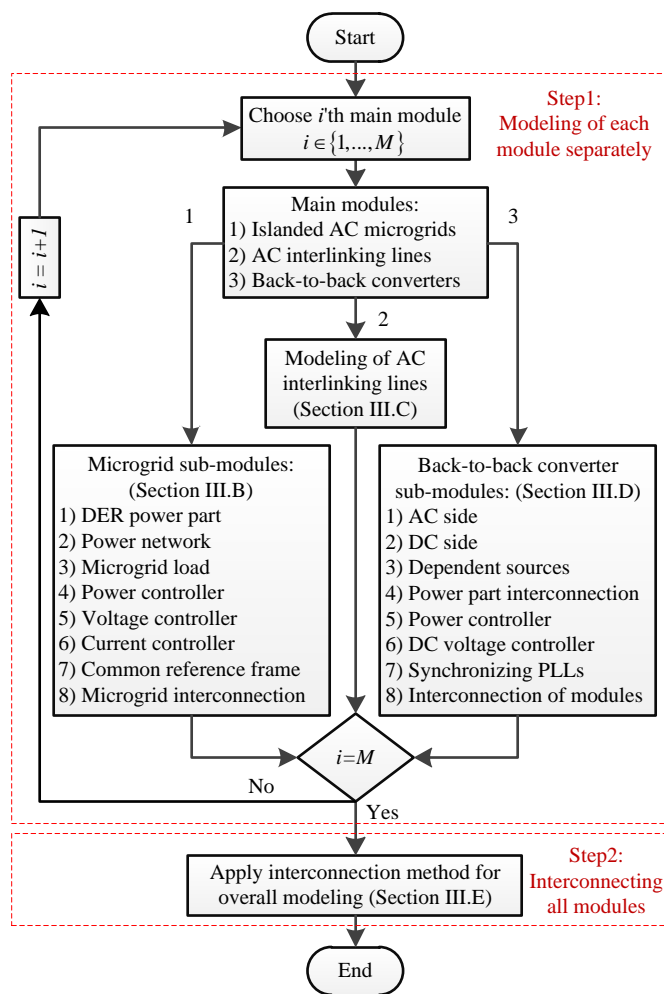


Fig. 2. Process of the proposed interconnection modeling method including two generic steps: modeling of each module separately and interconnecting all modules.

space model. The connections with other modules as shown in Fig. 1 typically for  $MG_i$ ,  $MG_j$ ,  $IL_{ij}$ ,  $IL_{ji}$  and  $BTBC_{ij}$  are considered in the model input/output. Interconnection process can be completed without more analytical calculation and only using RCT functions in MATLAB, which strongly reduces calculation burden/error. The RCT functions facilitate interconnecting a lot of sub-systems in order to model large-scale systems, e.g. IMGs.

In the case of IMGs modeling by the interconnection method 1) any number of separated modeled modules are transformed to system matrix form using *pck* function and are considered as sub-systems using *systemnames* function, 2) all inputs to the modules are specified using *input\_to* function, 3) the desired inputs and outputs for the overall model of IMGs are specified by *inputvar* and *outputvar* functions, 4) the overall model of IMGs is calculated by *sysic* function, and finally 5) it is transformed to state space representation by *unpck* function to be used in eigenvalue analysis. The details of the RCT functions in the general process of interconnecting the sub-systems are presented in [35].

Thus, modeling of any number of AC IMGs with different structures can be realized only by interconnecting the modules, i.e. MGs, BTBCs and AC ILs using the proposed interconnec-

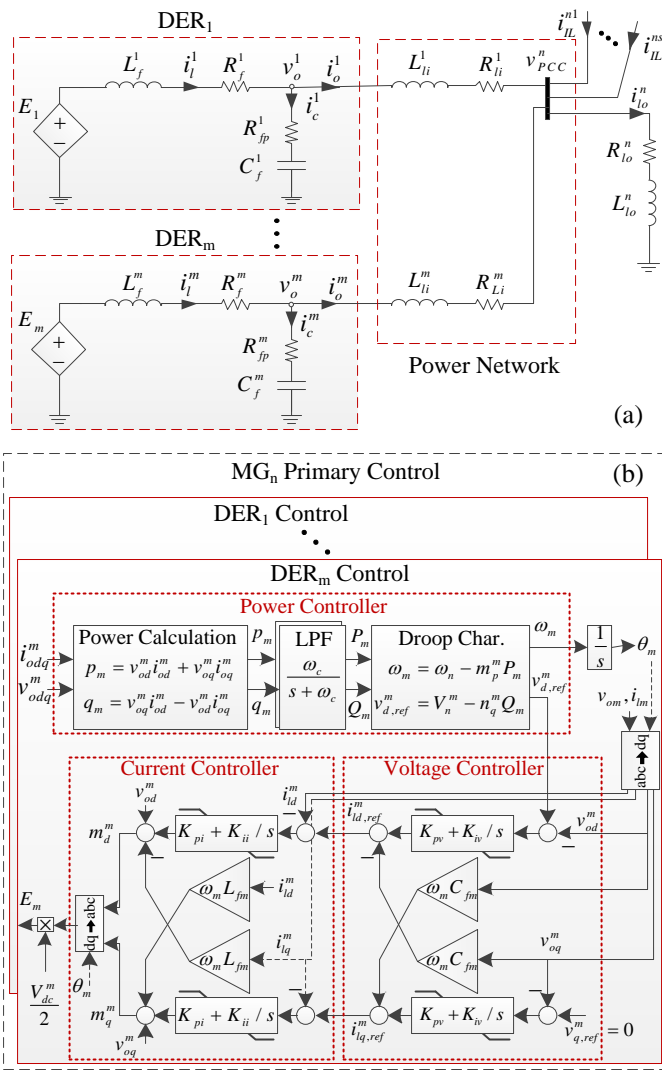


Fig. 3. A typical autonomous AC microgrid: (a) power part modules including voltage source converters, RLC filters, coupling lines and an integrated load, (b) primary control modules including power, voltage and current controllers.

tion method. Moreover, the interconnection method is used within modeling of each main module to further facilitate overall IMG modeling.

## B. Modeling of Autonomous Microgrids

In this paper, a uniform structure is considered for islanded MGs due to the ease of MG formulation expression and to focus on the IMG modeling. As shown in Fig. 3(a), the structure contains the basic elements of AC MGs, including DERs, RLC filters and lines. All DERs are assumed as ideal averaging modeled voltage source converters (VSCs) and a droop-based primary control is considered to share power among them as shown in Fig. 3(b).

1) *DER Power Part*: According to Fig. 3(a) and using circuit laws, Park transformation, and Taylor series-based linearization, the governing dynamic on the DER<sub>m</sub> power part, including the ideal voltage source and the RLC filter

are modeled as follows:

$$\begin{aligned} \Delta i_{ld}^m &= -(R_{fm}/L_{fm})\Delta i_{ld}^m + \omega_0 \Delta i_{lq}^m - (1/L_{fm})\Delta v_{od}^m \\ &\quad + (1/L_{fm})\Delta E_d^m + i_{lq0}^m \Delta \omega_m, \\ \Delta i_{lq}^m &= -\omega_0 \Delta i_{ld}^m - (R_{fm}/L_{fm})\Delta i_{lq}^m - (1/L_{fm})\Delta v_{oq}^m \\ &\quad + (1/L_{fm})\Delta E_q^m - i_{ld0}^m \Delta \omega_m, \\ \Delta v_{od}^m &= (1/C_{fm})i_{ld}^m + \omega_0 \Delta v_{oq}^m - (1/C_{fm})\Delta i_{od}^m + v_{oq0}^m \Delta \omega_m, \\ \Delta v_{oq}^m &= (1/C_{fm})i_{lq}^m - \omega_0 \Delta v_{od}^m - (1/C_{fm})\Delta i_{oq}^m - v_{od0}^m \Delta \omega_m, \end{aligned} \quad (1)$$

where  $E_d^m$  and  $E_q^m$  are the  $dq$ -components of  $E_m$ , 0 indicates a variable value at the equilibrium point and other parameters and variables are specified in Fig. 3. A state space representation of (1) can be given as follows:

$$\begin{aligned} \dot{X}_{DP}^m &= A_{DP}^m X_{DP}^m + B_{DP}^m U_{DP}^m + B_{PN}^m U_{PN}^m, \\ Y_{DP}^m &= C_{DP}^m X_{DP}^m + D_{DP}^m U_{DP}^m + D_{PN}^m U_{PN}^m, \end{aligned} \quad (2)$$

where  $X_{DP}^m = [\Delta i_{ld}^m \ \Delta v_{odq}^m]^T$ , the control input  $U_{DP}^m = [\Delta E_{dq}^m \ \Delta \omega_m]^T$ , the disturbance input  $U_{PN}^m = \Delta i_{odq}^m$ ,  $B_{PN}^m = [0_2 \ -(1/C_f^m)I_2]^T$ ,  $C_{DP}^m = I_4$ ,  $D_{DP}^m = 0_{4 \times 3}$ ,  $D_{PN}^m = 0_{4 \times 2}$

$$\begin{aligned} A_{DP}^m &= \begin{bmatrix} -R_f^m/L_f^m & \omega_0 & -1/L_f^m & 0 \\ -\omega_0 & -R_f^m/L_f^m & 0 & -1/L_f^m \\ 1/C_f^m & 0 & 0 & \omega_0 \\ 0 & 1/C_f^m & -\omega_0 & 0 \end{bmatrix}, \\ B_{DP}^m &= \begin{bmatrix} 1/L_f^m & 0 & i_{lq0}^m \\ 0 & 1/L_f^m & -i_{ld0}^m \\ 0 & 0 & v_{oq0}^m \\ 0 & 0 & -v_{od0}^m \end{bmatrix}. \end{aligned}$$

2) *Power Network*: Although any type of MG power network can be considered, here a common one, including linking lines from DERs to the point of common coupling (PCC) is assumed (see Fig. 3(a)). The dynamic model of the  $m$ 'th line of the power network is expressed as follows:

$$\begin{aligned} \Delta i_{od}^m &= -(R_{li}^m/L_{li}^m)\Delta i_{od}^m + \omega_0 \Delta i_{oq}^m + (1/L_{li}^m)\Delta v_{od}^m \\ &\quad - (1/L_{li}^m)\Delta v_{pcc,d}^m + v_{oq0}^m \Delta \omega_{com}^n, \\ \Delta i_{oq}^m &= -\omega_0 \Delta i_{od}^m - (R_{li}^m/L_{li}^m)\Delta i_{oq}^m + (1/L_{li}^m)\Delta v_{oq}^m \\ &\quad - (1/L_{li}^m)\Delta v_{pcc,q}^m - v_{od0}^m \Delta \omega_{com}^n, \end{aligned} \quad (3)$$

where  $\Delta \omega_{com}^n$  is the perturbed frequency form of the MG<sub>n</sub>'s common reference frame (CRF), which is explained in Section III-B7. Equation (3) is represented in a state space form as:

$$\begin{aligned} \dot{X}_{PL}^m &= A_{PL}^m X_{PL}^m + B_{LD}^m U_{LD}^m + B_{LP}^m U_{LP}^m + B_{Lw}^m U_{Lw}^m, \\ Y_{PL}^m &= C_{PL}^m X_{PL}^m, \end{aligned} \quad (4)$$

where,  $X_{PL}^m = Y_{PL}^m = \Delta i_{odq}^m$ ,  $U_{LP}^m = \Delta v_{pcc,dq}^m$ ,  $U_{LD}^m = Y_{DP}^m$ ,  $U_{Lw}^m = \Delta \omega_{com}^n$ , and matrices can be found using (3).

3) *MG Load*: In this paper, an integrated series RL load is assumed for each MG. Hence, the relationships for the MG<sub>n</sub> load dynamic in  $dq$  frame are similar to (3) and can be represented as a state space model:

$$\begin{aligned} \dot{X}_{ML}^n &= A_{ML}^n X_{ML}^n + B_{MLC}^n U_{MLC}^n + B_{MLP}^n U_{MLP}^n, \\ Y_{ML}^n &= C_{ML}^n X_{ML}^n, \end{aligned} \quad (5)$$

where  $X_{ML}^n = Y_{ML}^n = \Delta i_{lo,dq}^n$ ,  $U_{MLC}^n = \Delta \omega_{com}^n$ ,  $U_{MLP}^n = \Delta v_{pcc,dq}^n$ , and all matrices can be easily calculated.

Note that in the case of more loads and different power networks, (4) and (5) should be found for all lines and loads. Then, their connections can be realized by the method proposed in Section III-B8.

4) *Power Controller*: As shown in Fig. 3(b), the power controller of each DER consists of a power calculator, two LPFs, and  $\omega - P$  and  $V_d - Q$  droop characteristics. The droop characteristics are proportional controllers. Therefore, in order to find the small-signal model of the power controller, it is sufficient to consider the dynamics of LPFs and the integrator of the local voltage phase ( $\theta_m$ ) producer. According to the reason presented in Section III-B7, the angle difference of the DER<sub>m</sub>'s reference frame from the CRF ( $\delta_m$ ) is considered as a state variable instead of the  $\theta_m$  that is calculated as follows:

$$\delta_m = \theta_m - \theta_{com}^n = \int (\omega_m - \omega_{com}^n) dt, \quad (6)$$

where  $\omega_m$  is the DER<sub>m</sub> frequency and  $\theta_{com}^n$  is the voltage phase of the DER<sub>1</sub>, which the MG<sub>n</sub>'s CRF is based on it. Consequently, a state space representation is deduced as:

$$\begin{aligned} \dot{X}_{PC}^m &= A_{PC}^m X_{PC}^m + B_{PC}^m U_{PC}^m + B_{com}^m \Delta \omega_{com}^n, \\ Y_{PC}^m &= C_{PC}^m X_{PC}^m, \end{aligned} \quad (7)$$

where  $X_{PC}^m = [\Delta \delta_m \quad \Delta P_m \quad \Delta Q_m]^T$ ,  $U_{PC}^m = [Y_{DP}^m \quad Y_{PL}^m]^T$ ,  $Y_{PC}^m = [\Delta \omega_m \quad \Delta v_{dq,ref}^m \quad \Delta \delta_m]^T$ ,  $B_{PC}^m = [B_{PDP}^m \quad B_{PPL}^m]$  and

$$\begin{aligned} A_{PC}^m &= \begin{bmatrix} 0 & -m_p^m & 0 \\ 0 & -\omega_c & 0 \\ 0 & 0 & -\omega_c \end{bmatrix}, B_{PPL}^m = \begin{bmatrix} 0 & 0 \\ \omega_c v_{od0}^m & \omega_c v_{oq0}^m \\ -\omega_c v_{oq0}^m & \omega_c v_{od0}^m \end{bmatrix}, \\ B_{PDP}^m &= \begin{bmatrix} 0 & 0 & 0 & 0 \\ 0 & 0 & \omega_c i_{od0}^m & \omega_c i_{oq0}^m \\ 0 & 0 & \omega_c i_{oq0}^m & -\omega_c i_{od0}^m \end{bmatrix}, \\ C_{PC}^m &= \begin{bmatrix} 0 & -m_p^m & 0 \\ 0 & 0 & -n_q^m \\ 0 & 0 & 0 \\ 1 & 0 & 0 \end{bmatrix}, B_{com}^m = [-1 \quad 0 \quad 0]^T. \end{aligned}$$

5) *Voltage Controller*: Any DER in an autonomous MG has a voltage controller in order to regulate its output voltage. The  $d$ -component reference is received from the  $V_d - Q$  droop characteristic and the  $q$ -component reference is set to zero. Therefore, by considering a PI controller, as shown in Fig. 3(b), and considering the output of the integrators as the state variables ( $X_{VC}^m$ ), a state space representation can be given as:

$$\begin{aligned} \dot{X}_{VC}^m &= A_{VC}^m X_{VC}^m + B_{VC}^m U_{VC}^m, \\ Y_{VC}^m &= C_{VC}^m X_{VC}^m + D_{VC}^m U_{VC}^m, \end{aligned} \quad (8)$$

where  $U_{VC}^m = [Y_{DP}^m \quad Y_{PC}^m]^T$ ,  $Y_{VC}^m = i_{ldq}^{ref}$ ,  $A_{VC}^m = 0_2$ ,  $C_{VC}^m = I_2$ ,  $B_{VC}^m = [B_{VDP}^m \quad B_{VPC}^m]$ ,  $D_{VC}^m = [D_{VDP}^m \quad D_{VPC}^m]$ . The sub-matrices are as  $B_{VDP}^m = [0_2 \quad -K_{iv} I_2]$ ,  $B_{VPC}^m = [0_{2 \times 1} \quad K_{iv} I_2 \quad 0_{2 \times 1}]$ , and

$$\begin{aligned} D_{VPC}^m &= \begin{bmatrix} 0_{1 \times 2} & -K_{pv} & -\omega_0 C_f^m & 0_{1 \times 2} \\ 0_{1 \times 2} & \omega_0 C_f^m & -K_{pv} & 0_{1 \times 2} \end{bmatrix}, \\ D_{VDP}^m &= \begin{bmatrix} -C_f^m v_{oq0}^m & K_{pv} & 0 \\ C_f^m v_{od0}^m & 0 & K_{pv} \end{bmatrix}. \end{aligned}$$

6) *Current Controller*: A  $dq$ -frame PI current controller for DER<sub>m</sub> is shown in Fig. 3(b) in relation with the MG<sub>n</sub> primary control. By considering the outputs of integrators as state variables ( $X_{CC}^m$ ) and applying block diagram relationships, the state space model of the current controller is represented as:

$$\begin{aligned} \dot{X}_{CC}^m &= A_{CC}^m X_{CC}^m + B_{CC}^m U_{CC}^m, \\ Y_{CC}^m &= C_{CC}^m X_{CC}^m + D_{CC}^m U_{CC}^m, \end{aligned} \quad (9)$$

where  $U_{CC}^m = [Y_{DP}^m \quad Y_{VC}^m \quad \Delta \omega_m]^T$ ,  $Y_{CC}^m = m_{dq}^m$ ,  $A_{CC}^m = 0_2$ ,  $C_{CC}^m = I_2$ ,  $B_{CC}^m = [B_{CDP}^m \quad B_{CVC}^m \quad B_{CPC}^m]$  and  $D_{CC}^m = [D_{CDP}^m \quad D_{CVC}^m \quad D_{CPC}^m]$ . The sub-matrices are as  $B_{CDP}^m = [-K_{ii} I_2 \quad 0_2]$ ,  $B_{CVC}^m = K_{ii} I_2$ ,  $B_{CPC}^m = 0_{2 \times 3}$ ,  $D_{CVC}^m = K_{pi} I_2$ ,  $D_{CPC}^m = [-L_f^m i_{lq0}^m \quad L_f^m i_{ld0}^m]$  and

$$D_{CDP}^m = \begin{bmatrix} -K_{pi} & -\omega_{m0} L_f^m & 1 & 0 \\ \omega_{m0} L_f^m & -K_{pi} & 0 & 1 \end{bmatrix}.$$

7) *Common Reference Frame*: The DER frequency references are produced independently as shown in Fig. 3(b). Though the frequencies are equal in stable steady state operation, their dynamics can be different. Therefore, a CRF should be considered to model DER frequency interactions [10], [16], [23]. For this purpose, the following five steps are necessary.

i) One of the DER reference frames should be considered as the CRF. In this paper, the reference frame of the DER<sub>1</sub> of each MG is considered as the CRF.

ii)  $\Delta \delta$  is determined as a state variable of each DER, which is realized in the power controller (see Section III-B4).

iii)  $\omega_{com}$  is used in the modeling passive modules without self-produced frequency such as loads and power networks.

iv) The output variables of each individual reference frame to the modules, which are stated in the CRF, should be transformed to the CRF and vice versa. For instance, the  $v_{o,dq}^m$  is stated in the individual  $m$ 'th reference frame as an input to the power network, which is stated in the CRF. Hence, the  $v_{o,dq}^m$  should be transformed to the CRF. Similarly, the inverse transformation is needed for  $i_{odq}^m$ . Both the transformation and its inverse in a perturbed form are as follows:

$$\Delta v_{DQ} = T_s \cdot \Delta v_{dq} + T_{\delta 1} \cdot \Delta \delta, \quad (10a)$$

$$\Delta v_{dq} = T_s^{-1} \cdot \Delta v_{DQ} + T_{\delta 2} \cdot \Delta \delta, \quad (10b)$$

where the  $v_{DQ}$  and  $v_{dq}$  express variables in CRF and individual frames respectively, and

$$T_s = \begin{bmatrix} \cos \delta_0 & -\sin \delta_0 \\ \sin \delta_0 & \cos \delta_0 \end{bmatrix},$$

$$T_{\delta 1} = \begin{bmatrix} -(v_{d0} \sin \delta_0 + v_{q0} \cos \delta_0) \\ v_{d0} \cos \delta_0 - v_{q0} \sin \delta_0 \end{bmatrix},$$

$$T_{\delta 2} = \begin{bmatrix} -v_{d0} \sin \delta_0 + v_{q0} \cos \delta_0 \\ -(v_{d0} \cos \delta_0 + v_{q0} \sin \delta_0) \end{bmatrix}.$$

v) Since the MGs are interconnected by BTBCs, where the DC links make the MG frequencies independent, individual CRFs should be considered for MGs.

8) *MG Interconnection and Complete Model*: In order to find an inclusive state space representation for each MG, all partial module models presented in previous sub-sections should be interconnected. The input and output of each module



where  $X_{Bac}^i = Y_{Bac}^i = [\Delta i_{fc,dq}^i \ \Delta v_{fc,dq}^i]^T$ ,  $U_{Bac1}^i = [\Delta E_{Cdq}^i \ \Delta \omega_B^i]^T$ ,  $U_{Bac2}^i = \Delta I_{IL,dq}^{ij}$ , and the matrices are as

$$A_{Bac}^i = \begin{bmatrix} -R_{fc}^i/L_{fc}^i & \omega_{B0}^i & -1/L_{fc}^i & 0 \\ -\omega_{B0}^i & -R_{fc}^i/L_{fc}^i & 0 & -1/L_{fc}^i \\ 1/C_{fc}^i & 0 & 0 & \omega_{B0}^i \\ 0 & 1/C_{fc}^i & -\omega_{B0}^i & 0 \end{bmatrix},$$

$$B_{Bac1}^i = \begin{bmatrix} \frac{1}{L_{fc}^i} & 0 & i_{fc,q0}^i \\ 0 & \frac{1}{L_{fc}^i} & -i_{fc,d0}^i \\ 0 & 0 & v_{fc,q0}^i \\ 0 & 0 & -v_{fc,d0}^i \end{bmatrix}, B_{Bac2}^i = \begin{bmatrix} 0_2 \\ -(1/C_{fc}^i)I_2 \end{bmatrix}.$$

2) *DC Side*: The drawn currents by AC sides in order to form the dependent voltage sources, i.e.  $E_C^i$  and  $E_C^j$ , are modeled by current sources  $I_C^i$  and  $I_C^j$  shown in Fig. 5(b). In addition to the VSC's capacitors and series resistors, the DC line is modeled by a resistor in the BTBC DC side. One can easily find a state space representation as follows:

$$\begin{aligned} \dot{X}_{Bdc}^{ij} &= A_{Bdc}^{ij} X_{Bdc}^{ij} + B_{Bdc}^{ij} U_{Bdc}^{ij} \\ Y_{Bdc}^{ij} &= C_{Bdc}^{ij} X_{Bdc}^{ij} \end{aligned} \quad (15)$$

where  $X_{Bdc}^{ij} = [\Delta v_{dc}^i \ \Delta v_{dc}^j]^T$ ,  $U_{Bdc}^{ij} = [\Delta I_C^i \ \Delta I_C^j]^T$ , and

$$A_{Bdc}^{ij} = \begin{bmatrix} -1/(R_{dc}^{eq} C_{dc}^i) & 1/(R_{dc}^{eq} C_{dc}^i) \\ 1/(R_{dc}^{eq} C_{dc}^j) & -1/(R_{dc}^{eq} C_{dc}^j) \end{bmatrix},$$

$$B_{Bdc}^{ij} = \begin{bmatrix} (R_{dc}^i/R_{dc}^{eq}) - 1 & -(R_{dc}^j/R_{dc}^{eq}) \\ -(R_{dc}^i/R_{dc}^{eq}) & (R_{dc}^j/R_{dc}^{eq}) - 1 \end{bmatrix},$$

where  $R_{dc}^{eq} = R_{dc}^i + R_{dc}^j + R_{Ldc}^{ij}$ , and  $C_{Bdc}^{ij} = I_2$ .

3) *Dependent Current and Voltage Sources*: As shown in Fig. 5 (b), these sources are as transformations from AC/DC side to DC/AC side, which correlate both sides as follows:

$$\begin{aligned} I_C^i &= P_C^i/v_{dc}^i \\ E_C^i &= (1/2)m_i v_{dc}^i \end{aligned} \quad (16)$$

where  $P_C^i$  is the produced AC power of VSC<sub>i</sub> and  $m_i$  is the PWM control signal shown in Fig. 5(a). By linearizing (16), the transformations can be calculated as follows:

$$\begin{aligned} \Delta I_C^i &= T_{ac/dc}^i \begin{bmatrix} \Delta v_{dc}^i & \Delta E_{Cdq}^i & \Delta i_{fc,dq}^i \end{bmatrix}^T, \\ \Delta E_{Cdq}^i &= T_{dc/ac}^i \begin{bmatrix} \Delta v_{dc}^i & \Delta m_{dq}^i \end{bmatrix}^T, \end{aligned} \quad (17)$$

where

$$T_{ac/dc}^i = \frac{3}{2v_{dc0}^i} \begin{bmatrix} -\frac{2}{3}I_{C0}^i & E_{Cdq0}^i & E_{Cq0}^i & i_{fc,d0}^i & i_{fc,q0}^i \end{bmatrix}, \quad (18)$$

$$T_{dc/ac}^i = \frac{1}{2} \begin{bmatrix} m_{dq0}^i & v_{dc0}^i & 0 \\ m_{q0}^i & 0 & v_{dc0}^i \end{bmatrix}. \quad (19)$$

4) *BTBC Power Part Interconnection*: In order to simplify the BTBC modeling, the power part interconnections among AC and DC sides and independent voltage and current sources are fulfilled before the control modeling. Fig. 5(c) displays this interconnection, which consists of the BTBC power modules and their interconnections with each other and the outside. The state space representation is calculated readily using the interconnection method, which can be expressed as:

$$\begin{aligned} \dot{X}_{BP}^{ij} &= A_{BP}^{ij} X_{BP}^{ij} + B_{BP}^{ij} U_{BP}^{ij} \\ Y_{BP}^{ij} &= C_{BP}^{ij} X_{BP}^{ij} + D_{BP}^{ij} U_{BP}^{ij} \end{aligned} \quad (20)$$

where  $X_{BP}^{ij}$  is a  $10 \times 1$  vector, including the state variables of the AC and DC sides as  $X_{BP}^{ij} = [X_{Bac}^i \ X_{Bac}^j \ X_{Bdc}^{ij}]$  and

$$\begin{aligned} U_{BP}^{ij} &= [\Delta m_{dq}^i \ \Delta \omega_B^i \ \Delta m_{dq}^j \ \Delta \omega_B^j \ \Delta i_{IL,dq}^{ij} \ \Delta i_{IL,dq}^{ji}]^T, \\ Y_{BP}^{ij} &= [\Delta i_{fc,dq}^i \ \Delta i_{fc,dq}^j \ \Delta v_{dc}^j \ \Delta v_{fc,dq}^i \ \Delta v_{fc,dq}^j]^T. \end{aligned}$$

The matrices  $A_{BP}^{ij}$ ,  $B_{BP}^{ij}$ ,  $C_{BP}^{ij}$ , and  $D_{BP}^{ij}$  are calculated numerically for an input data using the RCT functions.

5) *Power Controller*: Here, a current control method is employed to control the BTBC power exchange. In this method, the power references  $P_{ref}^{ij}$  and  $Q_{ref}^{ij}$  are provided by the GCL. Then, the current references  $i_{dq,ref}^{ij}$  are calculated as follows [36]:

$$\begin{aligned} i_{d,ref}^{ij} &= 2P_{ref}^{ij}/3v_{fc}^i, \\ i_{q,ref}^{ij} &= 2Q_{ref}^{ij}/3v_{fc}^i. \end{aligned} \quad (21)$$

It is easy to obtain a state space model similar to the PI current controller model of DERs, i.e. (9) by considering the integrators outputs of the PI controllers as the state variables ( $X_{Bpc}^i$ ) as follows:

$$\begin{aligned} \dot{X}_{Bpc}^i &= A_{Bpc}^i X_{Bpc}^i + B_{Bpc}^i U_{Bpc}^i \\ Y_{Bpc}^i &= C_{Bpc}^i X_{Bpc}^i + D_{Bpc}^i U_{Bpc}^i \end{aligned} \quad (22)$$

where  $U_{Bpc}^i = [\Delta V_{PCC,dq}^i \ \Delta i_{fc,dq}^i \ \Delta i_{dq,ref}^i \ \Delta \omega_B^i]^T$ ,  $Y_{Bpc}^i = \Delta m_{dq}^i$ , the matrices are as  $A_{Bpc}^i = 0_2$ ,  $B_{Bpc}^i = [B_{Bpc1}^i \ B_{Bpc2}^i \ B_{Bpc3}^i \ B_{Bpc4}^i]$ ,  $C_{Bpc}^i = (2/V_{dc})I_2$ ,  $D_{Bpc}^i = [D_{Bpc1}^i \ D_{Bpc2}^i \ D_{Bpc3}^i \ D_{Bpc4}^i]$  and the sub-matrices are as  $B_{Bpc1}^i = 0_2$ ,  $B_{Bpc2}^i = -K_{Bp}^i I_2$ ,  $B_{Bpc3}^i = K_{Bi}^i I_2$ ,  $B_{Bpc4}^i = 0_{2 \times 1}$ ,  $D_{Bpc1}^i = (2/V_{dc})I_2$ ,  $D_{Bpc3}^i = (2K_{Bp}^i/V_{dc})I_2$ , and

$$\begin{aligned} D_{Bpc2}^i &= \frac{2}{V_{dc}} \begin{bmatrix} -K_{Bp}^i & -L_{fc}^i \omega_B^i \\ L_{fc}^i \omega_B^i & -K_{Bp}^i \end{bmatrix}, \\ D_{Bpc4}^i &= \frac{2}{V_{dc}} \begin{bmatrix} -L_{fc}^i i_{fc,q0}^i \\ L_{fc}^i i_{fc,d0}^i \end{bmatrix}. \end{aligned}$$

$K_{Bp}^i$  and  $K_{Bi}^i$  are the proportional and integral gains of the PI current controller and  $V_{dc}$  is the nominal DC link voltage.

6) *DC Voltage Controller*: In order to have a stable BTBC operation, the VSC<sub>j</sub> needs to exchange the same active power with the VSC<sub>i</sub> by applying  $-P_{ref}^{ij}$  as the active power reference. In addition, the DC voltage should be controlled through the same control signal. On the other hand, although the VSC<sub>j</sub>'s reactive power reference is free from the VSC<sub>i</sub>'s  $Q_{ref}^{ij}$ , usually references with equal magnitudes are interested. Therefore, power references of the VSC<sub>j</sub> are expressed as:

$$P_{ref}^{ji} = u_{dc} - P_{ref}^{ij}, \quad Q_{ref}^{ji} = -Q_{ref}^{ij}, \quad (23)$$

where  $u_{dc}$  is the control effort of the  $V_{dc}^j$  controller shown in Fig. 5(a). Thus the current references can be calculated by (21) and a state space can be represented for VSC<sub>j</sub> current controller similar to (22) as follows:

$$\begin{aligned} \dot{X}_{Bvc}^j &= A_{Bvc}^j X_{Bvc}^j + B_{Bvc}^j U_{Bvc}^j \\ Y_{Bvc}^j &= C_{Bvc}^j X_{Bvc}^j + D_{Bvc}^j U_{Bvc}^j \end{aligned} \quad (24)$$

where  $X_{Bvc}^j$  is a  $2 \times 1$  vector of the integrators outputs of the PI controllers. Since the current controller structure is the

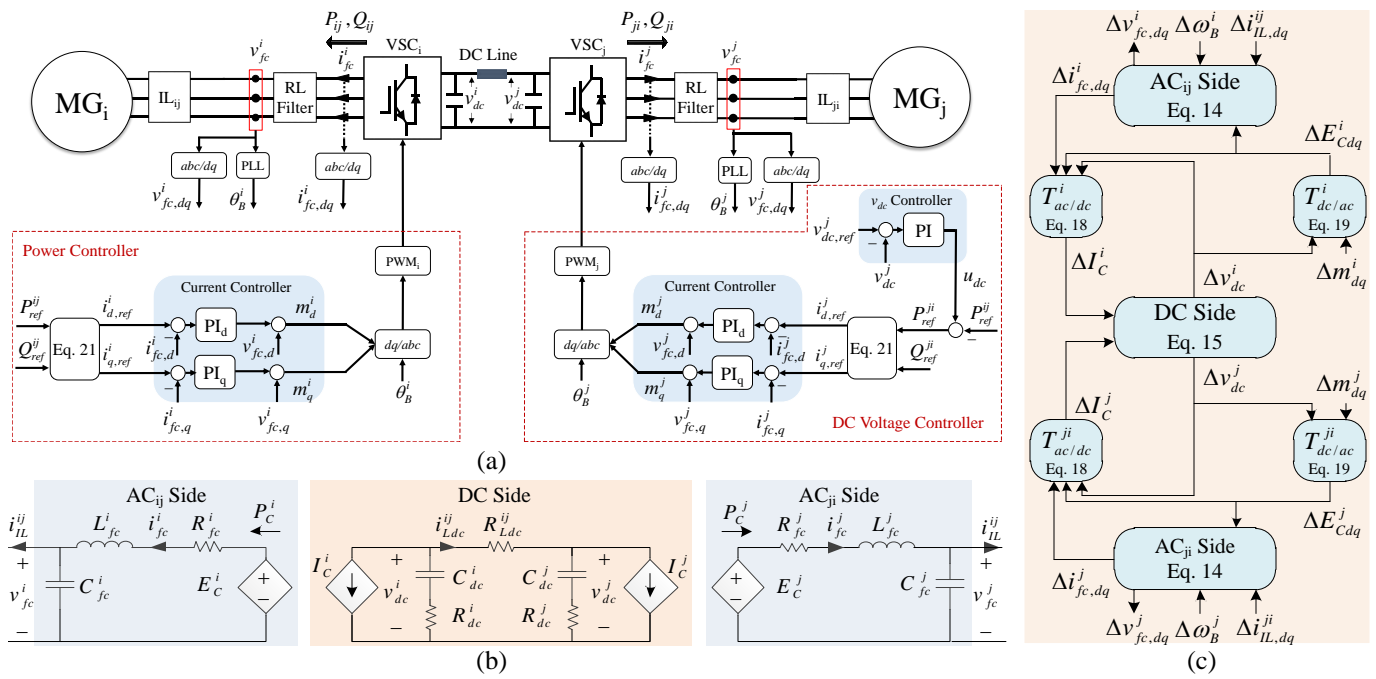


Fig. 5. Interlinking back-to-back converter: (a) control and operation block diagram, (b) power part averaging model, (c) power part interconnection.

same for the power controller and the DC voltage controller, input vector, output vector and all matrices and sub-matrices are equal to those of the BTBC power controller expressed below (22) with superscript  $j$ .

The  $V_{dc}^j$  controller, which is usually a PI controller is modeled using state space representation as follows:

$$\begin{aligned} \dot{X}_{DVC}^j &= B_{DVC}^j U_{DVC}^j, \\ Y_{DVC}^j &= C_{DVC}^j X_{DVC}^j + D_{DVC}^j U_{DVC}^j, \end{aligned} \quad (25)$$

where  $X_{DVC}^j$  is the integrator output,  $U_{DVC}^j = \Delta v_{dc}^j$ ,  $Y_{DVC}^j = \Delta i_{fc,d}^j$ ,  $B_{DVC}^j = K_i^{DVC}$ ,  $C_{DVC}^j = [2/3v_{fc,d}^i \ 0]^T$  and  $D_{DVC}^j = [2K_p^{DVC}/3v_{fc,d}^i \ 0]^T$ .  $K_p^{DVC}$  and  $K_i^{DVC}$  are the proportional and integral gains of the  $V_{dc}^j$  PI controller.

7) *Synchronizing PLLs*: As mentioned earlier, the BTBC needs two PLLs to synchronize AC sides with the MG's PCC voltages through ILs. The typical PLL structure is indicated in Fig. 6. An LPF is used to clear the  $v_{pcc,q}^i$  signal and a PI controller is used to enforce it to zero in order to lock  $\theta_B^i$  on the phase of  $v_{pcc}^i$ . Note that before enabling the BTBC to exchange the power,  $v_{fc}^i = v_{pcc}^i$ . Therefore, the  $v_{pcc}^i$  is measured by the  $v_{fc}^i$  transducer. In order to find the small-signal model of the PLL, PI and LPF integrator outputs are considered as state variables. Note that the third state variable is as  $\delta_B^i = \theta_B^i - \theta_{com}^i$  to state all BTBC AC side dynamics into the related CRF, e.g. VSC<sub>i</sub> dynamics state into the MG<sub>i</sub> CRF. Therefore, the state space representation is as follows:

$$\begin{aligned} \dot{X}_{PLL}^i &= A_{PLL}^i X_{PLL}^i + B_{PLL}^i U_{PLL}^i, \\ Y_{PLL}^i &= C_{PLL}^i X_{PLL}^i, \end{aligned} \quad (26)$$

where  $U_{PLL}^i = [\Delta v_{pcc,q}^i \ \Delta \omega_{com}^i]^T$ ,  $Y_{PLL}^i = [\Delta \omega_B^i \ \Delta \delta_B^i]$  and

$$B_{PLL}^i = \begin{bmatrix} 0 & \omega_c & 0 \\ 0 & 0 & -1 \end{bmatrix}^T, C_{PLL}^i = \begin{bmatrix} 1 & K_P^{PLL} & 0 \\ 0 & 0 & 1 \end{bmatrix},$$

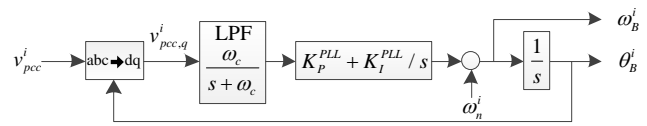


Fig. 6. The structure of phase-locked loop typically used for VSC<sub>i</sub>.

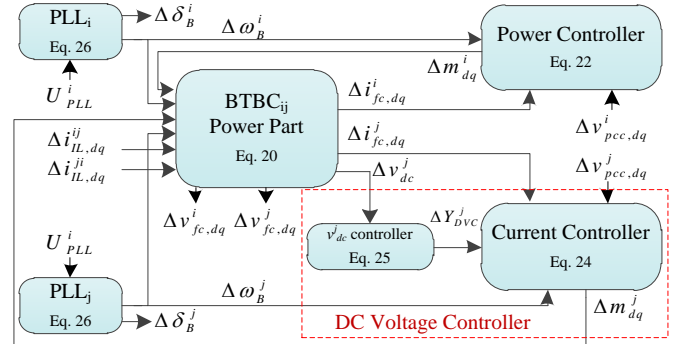


Fig. 7. Interconnections of power and control modules of the BTBC<sub>ij</sub>.

$$A_{PLL}^i = \begin{bmatrix} 0 & K_I^{PLL} & 0 \\ 0 & -\omega_c & 0 \\ 1 & K_P^{PLL} & 0 \end{bmatrix}.$$

8) *Complete Interconnection of BTBC Modules*: As the final step, the interconnections among all power and control modules represented by (20), (22), (24), (25) and (26) should be considered as shown in Fig. 7. The BTBC<sub>ij</sub> is modeled as:

$$\begin{aligned} \dot{X}_B^{ij} &= A_B^{ij} X_B^{ij} + B_B^{ij} U_B^{ij}, \\ Y_B^{ij} &= C_B^{ij} X_B^{ij} + D_B^{ij} U_B^{ij}, \end{aligned} \quad (27)$$

where  $X_B^{ij}$  is a  $21 \times 1$  state vector as

$$X_B^{ij} = [X_{BP}^{ij} \ X_{Bpc}^i \ X_{Bcc}^j \ X_{DVC}^j \ X_{PLL}^i \ X_{PLL}^j]^T.$$

By specifying the input and output vectors as  $U_B^{ij} = [\Delta v_{pcc,dq}^i \ \Delta i_{IL,dq}^{ij} \ \Delta v_{pcc,dq}^j \ \Delta i_{IL,dq}^{ji} \ \Delta \omega_{com}^i \ \Delta \omega_{com}^j]^T$  and  $Y_B^{ij} =$



$[\Delta v_{fc,dq}^i \Delta v_{fc,dq}^j \Delta v_{dc}^j \Delta \delta_B^i \Delta \delta_B^j]^T$ , considering the interconnections shown in Fig. 7 among all the BTBC modules, and using RCT functions in the interconnection method, the matrices can be calculated numerically for certain input data.

### E. Overall Interconnection of Interconnected Microgrids

By modeling all AC IMG modules, including AC MGs, BTBCs and AC/DC ILs, modeling of various structures of IMGs with any number of MGs and interconnections is possible using the interconnection method. Fig. 8 indicates the IMG interconnection focusing on the interconnection between  $MG_i$  and  $MG_j$  including  $BTBC_{ij}$ ,  $IL_{ij}$ ,  $IL_{ji}$ , and all modeling requirements (see Fig. 1). In fact,  $MG_i$ ,  $i = 1, \dots, n$  can be interlinked to all other MGs, e.g.  $MG_j$ ,  $j = 1, \dots, n$  and  $j \neq i$  through corresponding BTBCs and ILs, which shows the generality of the interconnection method.

Note that the MGs have independent CRFs, where their functional zones are shown in Fig. 8. All ILs and BTBC AC sides connected to each MG are covered by its CRF. Therefore, (10a) and (10b) are used for power interconnections between the MG/IL with the BTBC. The small-signal model can be represented in a free motion state space form as:

$$\dot{X}_{IMG} = A_{IMG} X_{IMG} \quad (28)$$

where  $X_{IMG}$  consists of the state variables of all participating modules in the IMGs and can be expressed as

$$X_{IMG} = [\underbrace{X_{MG}^1 \dots X_{MG}^n}_{MGs} \dots \underbrace{X_{IL}^{ij} \dots}_{ILs} \dots \underbrace{X_B^{ij} \dots}_{BTBCs}]^T,$$

including  $(13m + 2)n + 2p + 21q$  state variables, where  $n$ ,  $p$  and  $q$  are the number of MGs, ILs and BTBCs respectively.  $A_{IMG}$  can be expressed in a general form as:

$$A_{IMG} = [A_{rs}], \quad r, s = 1, \dots, t \quad (29)$$

where  $p$  is the number of all IMG modules and  $A_{rs} = \mathbf{0}$  when  $r \neq s$  and there is no direct connection between  $r$ 'th and  $s$ 'th modules, otherwise  $A_{rs} \neq \mathbf{0}$ .  $\mathbf{0}$  is a zero matrix with the appropriate size.

For each IMG case with certain data,  $A_{IMG}$  can be calculated numerically by considering the modules connections as generally shown in Fig. 8, and applying the interconnection method.

### F. Comparison with the Substitution Modeling Method

If the substituting method is employed for finding the complete MG model, the number of substituting can be found according to Fig. 4 and the output arrows from the equations blocks. By the left, (11) should be substituted in (4) for all  $m$  lines and in (5) for the load, which are totally  $m + 1$  substitutions. (5) should be substituted in (11), and (4) should be replaced in (10)(b) for all  $m$  lines without the coupling  $DER_1$  line ( $m$  substitution). (10)(b) is replaced in (2) and (7) for all DERs except  $DER_1$ , which the replacement is from (5) ( $2m$  substitutions). By substituting (2) in (7), (9) and (10)(a), (9) in (2), (8) in (9), and finally changed-dimension output of (7) in (2), (9) and (8),  $7m$  substitutions are required for all

DERs. The substitution process can be completed by replacing (10)(a) in (4) for all  $m$  lines except  $DER_1$  line, which the substituting is from (2) to (4) ( $m$  substitutions). All required manual substitutions are  $12m + 1$  that can be expressed as 13 when the similar substitutions are just considered as 1 substitution, i.e.  $m = 1$ .

A similar substituting process is needed for BTBCs using Figs. 5(c) and 7 that leads to 24 substitutions. Neglecting similar substitutions, required ones are reduced to 13.

According to Fig. 8, for each interconnection between two MGs, 20 substitutions (10 by neglecting the similar ones) are required. For  $n$  different autonomous AC MGs with  $k$  interconnections/BTBCs as shown in Fig. 8, totally  $\sum_{i=1}^n (12m_i + 1) + 44k$  substitutions (36 by neglecting the similar ones) are necessary to find the IMG model using the substitution method. Such a manual calculation process leads to a high calculation burden and may be accompanied by some errors. However, in the proposed interconnection method, the large number of substitutions are fulfilled numerically using the RCT functions with a low manual calculation burden only for specifying inputs of each module employing the pre-provided interconnections by Figs. 4, 5(c), 7, and 8. In fact, the calculation time/burden of the interconnection method can be determined as specifying the inputs of modules using *input\_to* function with respect to substituting the equations into each other in the substitution method. The number of specifying input vectors as a relatively time-consuming process is equal to the number of modules to be interconnected. Therefore, one can easily calculate it regarding Figs 4, 5(c), 7, and 8 as  $\sum_{i=1}^n (7m_i + 2) + 20k$ .

Note that both substitution and interconnection modeling methods lead to same results (e.g., from eigenvalue analysis or time-domain simulation), since both are based on the same module models and same strategy for selecting the input, output and state variables. The difference is only in the calculation burden and possible calculation errors.

Table I shows the calculation burden/error comparison for the common substitution method [14], [15] and the proposed interconnection method in two sample IMGs. In this comparison study,  $IMG_1$  is formed by three interconnected MGs through three BTBCs, where  $MG_1$  has three DERs,  $MG_2$  has four DERs, and  $MG_3$  has six DERs.  $IMG_2$  is composed of eight interconnected MGs through seven BTBCs, where each one of  $MG_1$ - $MG_3$  has two DERs, each one of  $MG_4$ - $MG_6$  has three DERs, and  $MG_7$  and  $MG_8$  consist of five and ten DERs, respectively. It is obvious that the number of substituting are larger than the number of specifying inputs in each case. Moreover, one can consider approximate average calculation times for specifying inputs as a fast manual process and substituting equations as a slow manual process as 30 seconds and 4 minutes, respectively. Hence, as shown in Table I, the total calculation time of substitution method for same case studies is much more than the corresponding time of the interconnection method. In addition, substituting equations may lead to different nested forms, which causes long calculation times or even manual calculation errors. However, specifying inputs is a straightforward MATLAB coding process without arithmetic complications.

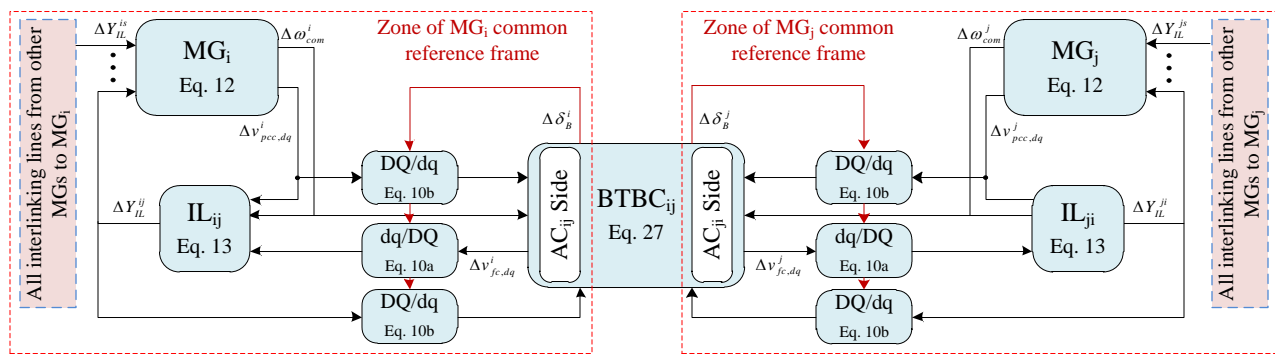


Fig. 8. Complete interconnection of AC microgrids focusing on the connection between  $MG_i$  and  $MG_j$  through  $IL_{ij}$ ,  $IL_{ji}$  and  $BTBC_{ij}$ .

TABLE I. COMPARISON OF THE COMMON SUBSTITUTION [14], [15] AND PROPOSED INTERCONNECTION METHODS

Modeling method	Possible manual error	Studied system	Number of substitution <i>input_to</i>	Manual calculation time (min)
Substitution	Module modeling and substituting	$IMG_1$	291	1164
		$IMG_2$	676	2704
Interconnection	Module modeling and input specifying	$IMG_1$	157	157
		$IMG_2$	366	366

#### IV. MODELING VALIDATION

Prony method is used for validating power system model in [32]. For this purpose, the small-signal model of the IMG is analyzed using eigenvalue analysis and participation matrix. Thus the participating eigenvalues and their contribution amount in each state variable can be determined. On the other hand, the waveform of each state variable obtained from the real system or a non-simplified model can be estimated using Prony method as a linear sum of damped complex exponentials [32]. The proposed modeling precision for each state variable is validated by comparing the participating eigenvalues and their contribution with the damped complex exponentials calculated by the Prony analysis [33]. In this paper, required input waveforms for Prony analysis are provided from real-time OPAL-RT simulator.

##### A. OPAL-RT Simulator

In order to indicate the practicality of real-time simulation for large-scale systems e.g. BTBC-IMGs, real-time software-in-the loop simulations are provided using OPAL-RT simulator. Fig. 9(a) shows the experimental setup located at Marine Microgrid Laboratory, Aalborg University including OPAL-RT simulator OP5600 as the target, the host PC, and a networking LAN cable. The OP5600 is configured with 4 activated Intel Xeon E5, 3.2 GHz processing cores, and works under Linux operating system. Moreover, it provides user-programmable I/O management, handled by a fast Xilinx Spartan-3 FPGA. The real-time simulation process is shown in Fig. 9(b). Version 11.2.1.91 of RT-LAB software is used as the interface between MATLAB and OPAL-RT digital simulator.

In order to simulate BTBC-IMGs as real time, the MATLAB/SimPowerSystems model is loaded on the OPAL-RT via the RT-LAB, then the real-time data is come back to the MATLAB environment inversely. The SimPowerSystems model should be divided into two subsystems, i.e. a subsystem comprising all permanent power and control parts during

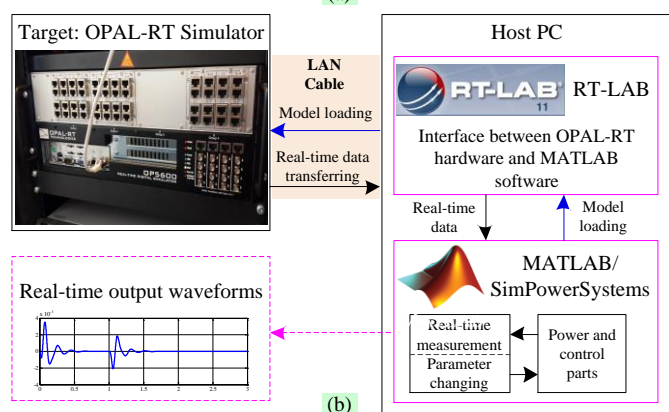
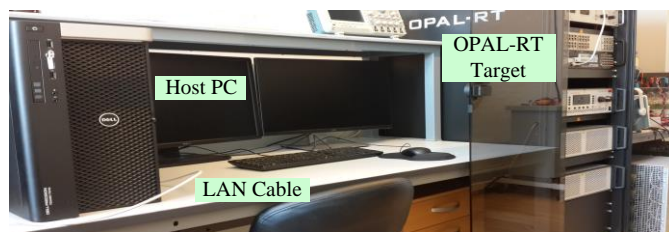


Fig. 9. (a) Real-time experimental setup including the OPAL-RT target, the host PC and a LAN cable for networking. (b) Real-time simulation process using OPAL-RT digital simulator.

the real-time simulation and a subsystem including displays and changeable parameters. After model loading and real-time data receiving, real-time waveforms can be measured in SimPowerSystems environment.

##### B. Interconnection Method Validation Using Prony Analysis

The introduced Prony analysis-based validation method is used for BTBC-IMGs. Due to lack of space the details are not given here. The two BTBC-IMGs introduced in Part II of the paper [37] is simulated as real-time using OPAL-RT simulator. The waveforms of OPAL-RT output and Prony analysis estimation are shown in Fig. 10 for  $\Delta\delta_2^{MG1}$ ,  $\Delta P_1^{MG2}$  and  $\Delta X_{DVC}$ , where generally  $\Delta x = x_{ref} - x$ ,  $\Delta x$  is the perturbed form of the state variable ( $x$ ) and  $x_{ref}$  is the reference value. The Prony method estimates the perturbed form of waveforms for a certain set-point, which is 850 W active power flow from  $MG_2$  to  $MG_1$  at  $t = 1$  s due to a power deficiency in  $MG_1$ . The data window shows the time interval of Prony estimation. All three waveforms show appropriate estimation by Prony analysis.

Comparative results for the estimated state variables are shown in Table II, where the eigenvalues and participation

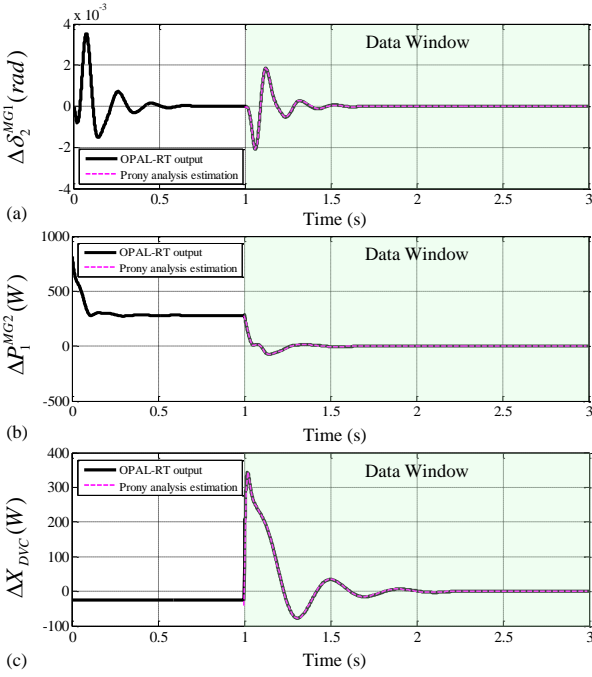


Fig. 10. Prony analysis-based estimation for perturbed form of OPAL-RT output waveforms: (a) the angle difference of the DER<sub>2</sub> reference frame from the common reference frame of MG<sub>1</sub>, (b) DER<sub>1</sub> active power of MG<sub>2</sub>, (c) integrator output of the DC voltage controller.

TABLE II. PRONY ANALYSIS-BASED MODEL VALIDATION

State variable	Eigenvalue	MVE (%)	Participation factor	MVE (%)
$\Delta\delta_2^{MG1}$	$-8 \pm j28.8$	5	0.96	8
	$-145 \pm j106$	8	0.03	3
$\Delta P_1^{MG2}$	$-8 \pm j28.8$	3	0.66	6
	-21.46	7	0.02	21
	-20	0	0.29	9
$\Delta X_{DVC}$	$-2 \pm j13.8$	6	0.45	3
	$-108 \pm j87$	8	0.55	3

factors are also calculated for the two BTBC-IMGs. The model validation error (MVE) indicates the difference between estimated modes (by Prony analysis) and calculated eigenvalues (by eigenvalue analysis) in the third column, and it shows the difference between normalized estimated amplitudes of the modes and participation factors (calculated by participation matrix) in the fifth column. In the first case, the MVE is calculated as relative error percentage:

$$MVE = \frac{|\gamma - \lambda|}{|\lambda|} \times 100, \quad (30)$$

where  $\gamma$  is a complex conjugate/real mode estimated by Prony analysis and  $\lambda$  is the correlated eigenvalue calculated via eigenvalue analysis. In the second case, the MVE is also calculated through (30), while  $\gamma$  is the normalized estimated amplitude and  $\lambda$  is the correlated participation factor.

The MVE is less than 10 % in all cases except  $\lambda = -21.46$ , which is not an effective dominant mode based on its participation factor, i.e. 0.02. Note that the presented Prony-based validation is able to be employed for all state variables.

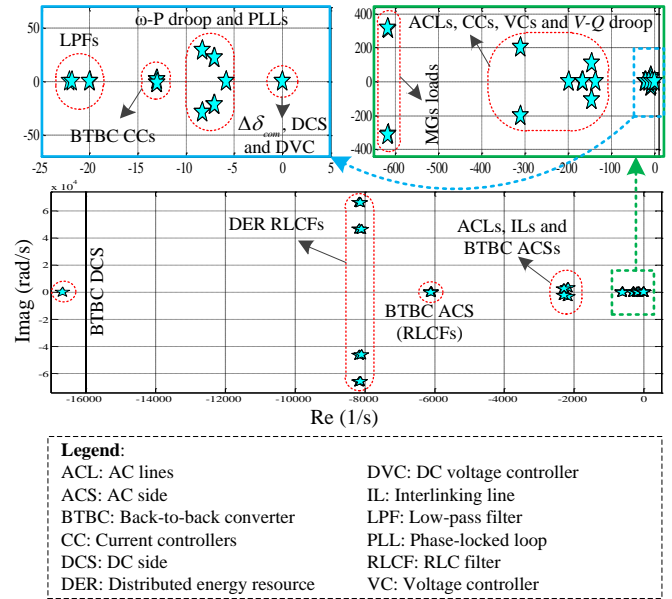


Fig. 11. All eigenvalues of the two interconnected microgrids.

## V. EIGENVALUE ANALYSIS RESULTS

As mentioned the required information for simulation is presented in Part II of the paper [37]. Fig. 11 shows all eigenvalues of the two IMGs through one BTBC, where the corresponding modules to each eigenvalue cluster are indicated generally using the participation matrix. The eigenvalues around -5000 real to -8000 real are mostly affected by DER and BTBC RLC filters. The eigenvalues between -2000 real and -3000 real are due to the AC lines, ILs and BTBC AC sides. More dominant modes can be categorized to the three clusters. The cluster near to -600 real is due to the MG loads. The eigenvalues cluster between -100 real and -350 real generally indicates the dynamic participation of the AC lines, DER current controllers, DER voltage controllers and  $V - Q$  droop characteristics. The dominant critical modes (third cluster) are related to the LPFs, BTBC current controllers, BTBC PLLs,  $\omega - P$  droop characteristics, DC side, DC voltage controller and  $\Delta\delta_{com}$ , which show the considerable BTBC impact on the IMG stability.

## VI. CONCLUSION

This paper has investigated the small-signal modeling of fully power-electronics based interconnected autonomous AC microgrids comprising VSC-based DERs and back-to-back converters exchanging power. For this purpose, the detailed module models are obtained, and their interconnections are realized employing convenient functions of robust control toolbox in MATLAB. The presented small-signal model is comprehensive and can be easily generalized for each number of autonomous AC MGs due to the expandability feature of the proposed interconnection method. It is validated using a Prony method and real-time simulation results, where the state variables are compared with their waveforms simulated in OPAL-RT simulator. Although, the validation is presented only for three state variables, each state variable within the model can be validated in the same way. Most effective state variables/modules on the critical modes show a remarkable

effect of back-to-back converters on the stability of interconnected autonomous microgrids. More conclusion are given in Part II of this work based on sensitivity analysis and time domain simulations.

### REFERENCES

[1] H. Bevrani, B. François, and T. Ise, *Microgrid dynamics and control*. John Wiley & Sons, 2017.

[2] C. Chen, J. Wang, F. Qiu, and D. Zhao, "Resilient distribution system by microgrids formation after natural disasters," *IEEE Trans. Smart Grid*, vol. 7, no. 2, pp. 958–966, 2016.

[3] M. Shahidehpour, Z. Li, S. Bahramirad, Z. Li, and W. Tian, "Networked microgrids: Exploring the possibilities of the it-bronzeville grid," *IEEE Power and Energy Mag.*, vol. 15, no. 4, pp. 63–71, 2017.

[4] E. Bullich-Massagué and et al., "Microgrid clustering architectures," *Applied Energy*, vol. 212, pp. 340–361, 2018.

[5] S. Moayedi and A. Davoudi, "Distributed tertiary control of dc microgrid clusters," *IEEE Trans. Power Electron.*, vol. 31, no. 2, pp. 1717–1733, 2016.

[6] Q. Shafiee, T. Dragičević, J. C. Vasquez, and J. M. Guerrero, "Hierarchical control for multiple dc-microgrids clusters," *IEEE Trans. Energy Conv.*, vol. 29, no. 4, pp. 922–933, 2014.

[7] E. Pashajavid, A. Ghosh, and F. Zare, "A multimode supervisory control scheme for coupling remote droop-regulated microgrids," *IEEE Trans. Smart Grid*, vol. 9, no. 5, pp. 5381–5392, 2018.

[8] L. Che, M. Shahidehpour, A. Alabdulwahab, and Y. Al-Turki, "Hierarchical coordination of a community microgrid with ac and dc microgrids," *IEEE Trans. Smart Grid*, vol. 6, no. 6, pp. 3042–3051, 2015.

[9] M. J. Hossain, M. A. Mahmud, F. Milano, S. Bacha, and A. Hably, "Design of robust distributed control for interconnected microgrids," *IEEE Trans. Smart Grid*, vol. 7, no. 6, pp. 2724–2735, 2016.

[10] I. P. Nikolakakos and et al., "Stability evaluation of interconnected multi-inverter microgrids through critical clusters," *IEEE Trans. Power Syst.*, vol. 31, no. 4, pp. 3060–3072, 2016.

[11] R. Zamora and A. K. Srivastava, "Multi-layer architecture for voltage and frequency control in networked microgrids," *IEEE Trans. Smart Grid*, vol. 9, no. 3, pp. 2076–2085, 2018.

[12] M. S. Golsorkhi, D. J. Hill, and H. R. Karshenas, "Distributed voltage control and power management of networked microgrids," *IEEE J. Emerging and Sel. Topics in Power Electron.*, vol. 6, no. 4, pp. 1892–1902, 2018.

[13] P. C. Loh, D. Li, Y. K. Chai, and F. Blaabjerg, "Autonomous operation of hybrid microgrid with ac and dc subgrids," *IEEE trans. power electron.*, vol. 28, no. 5, pp. 2214–2223, 2013.

[14] X. Wu, Y. Xu, X. Wu, J. He, J. M. Guerrero, C.-C. Liu, K. P. Schneider, and D. T. Ton, "A two-layer distributed control method for islanded networked microgrid systems," *IEEE Trans. Smart Grid*, to be published.

[15] Z. Zhao, P. Yang, Y. Wang, Z. Xu, and J. M. Guerrero, "Dynamic characteristics analysis and stabilization of pv-based multiple microgrid clusters," *IEEE Trans. Smart Grid*, to be published.

[16] F. Shahnian and A. Arefi, "Eigenanalysis-based small signal stability of the system of coupled sustainable microgrids," *Int. J. Electr. Power & Energy Syst.*, vol. 91, pp. 42–60, 2017.

[17] H.-J. Yoo, T.-T. Nguyen, and H.-M. Kim, "Multi-frequency control in a stand-alone multi-microgrid system using a back-to-back converter," *Energies*, vol. 10, no. 6, pp. 1–18, 2017.

[18] I. U. Nutkani, P. C. Loh, and F. Blaabjerg, "Distributed operation of interlinked ac microgrids with dynamic active and reactive power tuning," *IEEE trans. ind. appl.*, vol. 49, no. 5, pp. 2188–2196, 2013.

[19] C.-Y. Tang, Y.-F. Chen, Y.-M. Chen, and Y.-R. Chang, "Dc-link voltage control strategy for three-phase back-to-back active power conditioners," *IEEE Trans. Ind. Electron.*, vol. 62, no. 10, pp. 6306–6316, 2015.

[20] J. Suh, D.-H. Yoon, Y.-S. Cho, and G. Jang, "Flexible frequency operation strategy of power system with high renewable penetration," *IEEE Trans. Sustainable Energy*, vol. 8, no. 1, pp. 192–199, 2017.

[21] R. Majumder and G. Bag, "Parallel operation of converter interfaced multiple microgrids," *Int. J. Electr. Power & Energy Syst.*, vol. 55, pp. 486–496, 2014.

[22] R. Majumder, A. Ghosh, G. Ledwich, and F. Zare, "Power management and power flow control with back-to-back converters in a utility connected microgrid," *IEEE Trans. Power Syst.*, vol. 25, no. 2, pp. 821–834, 2010.

[23] N. Pogaku, M. Prodanovic, and T. C. Green, "Modeling, analysis and testing of autonomous operation of an inverter-based microgrid," *IEEE Trans. Power Electron.*, vol. 22, no. 2, pp. 613–625, 2007.

[24] N. Bottrell, M. Prodanovic, and T. C. Green, "Dynamic stability of a microgrid with an active load," *IEEE Trans. Power Electron.*, vol. 28, no. 11, pp. 5107–5119, 2013.

[25] A. Kahrobaei and Y. A.-R. I. Mohamed, "Analysis and mitigation of low-frequency instabilities in autonomous medium-voltage converter-based microgrids with dynamic loads," *IEEE Trans. Ind. Electron.*, vol. 61, no. 4, pp. 1643–1658, 2013.

[26] I. P. Nikolakakos, H. Zeineldin, M. S. El-Moursi, and J. L. Kirtley, "Reduced-order model for inter-inverter oscillations in islanded droop-controlled microgrids," *IEEE Trans. Smart Grid*, vol. 9, no. 5, pp. 4953–4963, 2017.

[27] M. Naderi, Y. Khayat, Q. Shafiee, H. Bevrani, and F. Blaabjerg, "Modeling of islanded microgrids using static and dynamic equivalent thevenin circuits," in *2018 20th IEEE Euro. Conf. on Power Electron. and Appl. (EPE'18 ECCE Europe)*, 2018, pp. 1–10.

[28] Y. Khayat, M. Naderi, Q. Shafiee, Y. Batmani, M. Fathi, J. M. Guerrero, and H. Bevrani, "Decentralized optimal frequency control in autonomous microgrids," *IEEE Trans. Power Syst.*, vol. 34, no. 3, pp. 2345–2353, 2018.

[29] Z. Shuai, Y. Peng, X. Liu, Z. Li, J. M. Guerrero, and Z. J. Shen, "Dynamic equivalent modeling for multi-microgrid based on structure preservation method," *IEEE Trans. Smart Grid*, 2018, DOI: 10.1109/TSG.2018.2844107.

[30] F. Shahnian, "Stability and eigenanalysis of a sustainable remote area microgrid with a transforming structure," *Sustainable Energy, Grids and Netw.*, vol. 8, pp. 37–50, 2016.

[31] Y. Zhang, L. Xie, and Q. Ding, "Interactive control of coupled microgrids for guaranteed system-wide small signal stability," *IEEE Trans. Smart Grid*, vol. 7, no. 2, pp. 1088–1096, 2016.

[32] S. Jiang, U. Annakkage, and A. Gole, "A platform for validation of facts models," *IEEE Trans. Power Del.*, vol. 21, no. 1, pp. 484–491, 2006.

[33] H. Golpira, M. R. Haghifam, and H. Seifi, "Dynamic power system equivalence considering distributed energy resources using prony analysis," *Int. Trans. Electr. Energy Syst.*, vol. 25, no. 8, pp. 1539–1551, 2015.

[34] Q. Shafiee, J. M. Guerrero, and J. C. Vasquez, "Distributed secondary control for islanded microgrids—a novel approach," *IEEE Transactions on power electronics*, vol. 29, no. 2, pp. 1018–1031, 2013.

[35] G. J. Balas, J. C. Doyle, K. Glover, A. Packard, and R. Smith,  *$\mu$ -analysis and synthesis toolbox: for use with Matlab*. The MathWorks Inc., 1994.

[36] A. Yazdani and R. Iravani, *Voltage-sourced converters in power systems*. Wiley Online Library, 2010, vol. 34.

[37] M. Naderi, Y. Khayat, Q. Shafiee, T. Dragicevic, H. Bevrani, and F. Blaabjerg, "Interconnected autonomous ac microgrids via back-to-back converters—part II: Stability analysis," *IEEE Trans. Power Electron.*, under review.



**Mobin Naderi** (S'16) was born in Paveh, Iran. He received the B.Sc. and M.Sc. degrees in Electrical Engineering from Tabriz University, Tabriz, Iran, in 2012 and Iran University of Science and Technology, Tehran, Iran, in 2014. He was a Visiting PhD student with Department of Energy Technology, Aalborg University, Aalborg, Denmark. He is now working toward the Ph.D. degree in the control of power systems at the University of Kurdistan, Iran. His research interests focus on robust control methods, and modeling, stability and control of autonomous and interconnected AC microgrids.



**Yousef Khayat** (S'16) received the B.Sc. degree from Urmia University, Urmia, Iran, and the M.Sc. degree (with Hons.) from Iran University of Science and Technology (IUST), Tehran, Iran, both in Electrical Engineering in 2012 and 2014, respectively. He is working toward the Ph.D. degree in control of power systems at the University of Kurdistan, Iran. He is also currently a Ph.D. Visiting Student with Aalborg University, Aalborg, Denmark. His research interests include Microgrid dynamics and control, robust, predictive and nonlinear control for application of power electronics in distributed systems.



**Qobad Shafiee** (S'13–M'15–SM'17) received PhD degree in electrical engineering from the Department of Energy Technology, Aalborg University (Denmark) in 2014. He is currently an Assistant Professor, Associate Director of International Relations, and the Program Co-Leader of the Smart/Micro Grids Research Center at the University of Kurdistan, Sanandaj, Iran, where he was a lecturer from 2007 to 2011. In 2014, he was a Visiting Scholar with the Electrical Engineering Department, the University of Texas at Arlington, Arlington,

TX, USA. He was a Post-Doctoral Fellow with the Department of Energy Technology, Aalborg University in 2015. His current research interests include modeling, energy management, control of power electronics-based systems and microgrids, and model predictive and optimal control of modern power systems.



**Frede Blaabjerg** (S'86 - M'88 - SM'97 - F'03) was with ABB-Scandia, Randers, Denmark, from 1987 to 1988. From 1988 to 1992, he got the PhD degree in Electrical Engineering at Aalborg University in 1995. He became an Assistant Professor in 1992, an Associate Professor in 1996, and a Full Professor of power electronics and drives in 1998. From 2017 he became a Villum Investigator. He is honoris causa at University Politehnica Timisoara (UPT), Romania and Tallinn Technical University (TTU) in Estonia. His current research interests include

power electronics and its applications such as in wind turbines, PV systems, reliability, harmonics and adjustable speed drives. He has published more than 600 journal papers in the fields of power electronics and its applications. He is the co-author of four monographs and editor of ten books in power electronics and its applications. He has received 30 IEEE Prize Paper Awards, the IEEE PELS Distinguished Service Award in 2009, the EPE-PEMC Council Award in 2010, the IEEE William E. Newell Power Electronics Award 2014 and the Villum Kann Rasmussen Research Award 2014. He was the Editor-in-Chief of the IEEE TRANSACTIONS ON POWER ELECTRONICS from 2006 to 2012. He has been Distinguished Lecturer for the IEEE Power Electronics Society from 2005 to 2007 and for the IEEE Industry Applications Society from 2010 to 2011 as well as 2017 to 2018. In 2019-2020 he serves a President of IEEE Power Electronics Society. He is Vice-President of the Danish Academy of Technical Sciences too. He is nominated in 2014-2018 by Thomson Reuters to be between the most 250 cited researchers in Engineering in the world.



**Tomislav Dragičević** received the M.Sc. and the industrial Ph.D. degrees in Electrical Engineering from the Faculty of Electrical Engineering, Zagreb, Croatia, in 2009 and 2013, respectively. From 2013 until 2016 he has been a Postdoctoral research associate at Aalborg University, Denmark. From March 2016 he is an Associate Professor at Aalborg University, Denmark where he leads an Advanced Control Lab.

He made a guest professor stay at Nottingham University, UK during spring/summer of 2018. His

principal field of interest is design and control of microgrids, and application of advanced modeling and control concepts to power electronic systems. He has authored and co-authored more than 180 technical papers (more than 80 of them are published in international journals, mostly IEEE Transactions) in his domain of interest, 8 book chapters and a book in the field.

He serves as Associate Editor in the IEEE TRANSACTIONS ON INDUSTRIAL ELECTRONICS, in IEEE Emerging and Selected Topics in Power Electronics and in IEEE Industrial Electronics Magazine. Dr. Dragičević is a recipient of the Končar prize for the best industrial PhD thesis in Croatia, and a Robert Mayer Energy Conservation award.



**Hassan Bevrani** (S'90 - M'04 - SM'08) received PhD degree in electrical engineering from Osaka University (Japan) in 2004. Currently, he is a full professor and the Program Leader of Smart/Micro Grids Research Center (SMGRC) at the University of Kurdistan (UOK). From 2016 to 2019 he was the UOK vice-chancellor for research and technology. Over the years, he has worked as senior research fellow and visiting professor with Osaka University, Kumamoto University (Japan), Queensland University of Technology (Australia), Kyushu Institute of

Technology (Japan), Centrale Lille (France), and Technical University of Berlin (Germany). Prof. Bevrani is the author of 6 international books, 15 book chapters, and more than 300 journal/conference papers. His current research interests include smart grid operation and control, power systems stability and optimization, Microgrid dynamics and control, and Intelligent/robust control applications in power electric industry.